Int J Fract (2012) 174:61–74
DOI 10.1007/s10704-011-9672-0

ORIGINAL PAPER

On configurational forces at boundaries in fracture mechanics

F. D. Fischer · N. K. Simha · J. Predan · R. Schöngrundner · O. Kolednik

Received: 5 August 2011 / Accepted: 20 December 2011 / Published online: 25 January 2012

Abstract Configurational forces invariably appear at the external boundaries of cracked bodies (including the crack faces), but it is unclear whether they influence crack growth. Also, it is unclear how such boundary configurational forces are related to the J-integrals calculated in the body. In this brief note, we (i) derive expressions for the surface configurational forces and determine their values on regions of the external boundaries with prescribed tractions or displacements, (ii) determine the relation between the far-field J-integral and the surface configurational forces, and (iii) show that surface configurational forces on the crack faces do not alter the relation between the near-tip and far-field J-integrals.

Keywords Configurational forces · External boundaries · Role of crack faces · J-integral vector · Analytical solutions · Finite element modeling

F. D. Fischer (✉)
Institute of Mechanics, Montanuniversität Leoben, Franz-Josef-Strasse 18, 8700 Leoben, Austria
e-mail: mechanik@unileoben.ac.at

N. K. Simha
Department of Biomedical Engineering, University of Minnesota, 312 Church St. S.E., Minneapolis, MN 55455, USA

J. Predan
Faculty of Mechanical Engineering, University of Maribor, Smetanova 17, 2000, Maribor, Slovenia

R. Schöngrundner
Materials Center Leoben Forschung GmbH, Roseggerstrasse 12, 8700 Leoben, Austria

O. Kolednik
Erich Schmid Institute of Materials Science, Austrian Academy of Sciences, Jahnstrasse 12, 8700 Leoben, Austria

Present Address:
N. K. Simha
Medtronic Inc., 710 Medtronic Parkway, Fridley, MN, 55432-5604, USA

1 Introduction

Configurational stresses and forces are now well-established quantities in fracture mechanics, see e.g. the books and articles by Maugin (1993, 1995, 2010), Gurtin (2000) and Kienzler and Herrmann (2000). In particular, configurational forces provide a convenient framework for studying shielding (or anti-shielding) of cracks due to material inhomogeneities, eigenstrain fields, plasticity, etc., see e.g. Simha et al. (2003, 2005, 2008), Kolednik et al. (2010) and references therein.

It is well known that configurational forces invariably appear at the external boundaries of any loaded body, see the example presented in Fig. 1, a linear-elastic plate containing a hole subjected to uniform, uniaxial tension. Such surface configurational forces can be viewed as driving forces for phenomena that can cause the external boundary to move in the reference configuration resulting in changes of the shape of

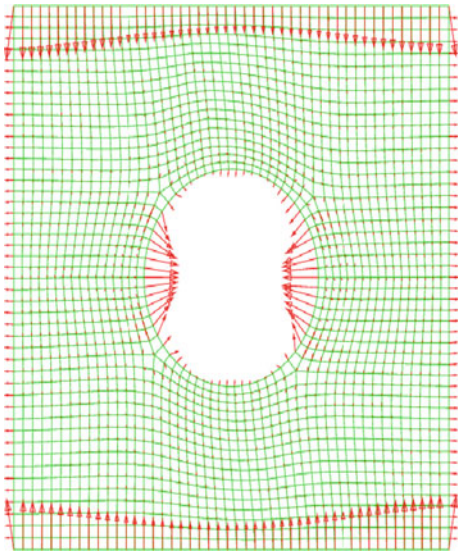

Fig. 1 Homogeneous linear-elastic plate containing a hole, subjected to uniform tension in the vertical direction. Configurational surface forces $\mathbf{f}_s$ appear at all the external boundaries. The far-field J-integral vector $\mathbf{J}_{far}$ is zero here, since the integral of $\mathbf{f}_s$ over the entire external boundary vanishes, see Eq. (22). The deformed configuration is shown, and configurational body forces appear at internal nodes, because the numerical implementation satisfies $\nabla \cdot \mathbf{S} = \mathbf{0}$ in the interior, but not $\nabla \cdot \mathbf{C} = \mathbf{0}$

the body by diffusion, or either loss of material or accumulation of new material by electrochemical processes, such as corrosion. It is clear that such processes may also influence the propagation of cracks in materials, but the subject of the current paper is a different problem: In elastic-plastic fracture mechanics, the near-tip J-integral is most often applied for characterizing the crack driving force or the intensity of the stress and strain field at the crack tip. It has been demonstrated that the J-integral is path independent for a homogeneous body with a stationary crack and traction-free crack faces, Rice (1968). This path dependence is very important for the application of the J-integral, since the evaluation of the J-integral directly at the crack tip is in most cases not possible. The magnitude of the J-integral, evaluated along a certain contour around the crack tip, and its path dependence are intimately related to the distribution of configurational forces in the body, see e.g. Simha et al. (2005, 2008). So it is not clear *a priori* whether surface configurational forces can be ignored in all fracture mechanics calculations. In particular, it is unclear whether the surface configurational forces on the crack faces influence the path dependence of the J-integral. Such surface configurational forces have been neglected in almost all applications of configurational forces for fracture mechanics so far.

The goal of this paper is to determine the role of the surface configurational forces on the external boundaries of fracture mechanics specimens. In Sect. 2, we derive the expressions for the surface configurational forces. In Sect. 3, we determine the influence of the surface configurational forces on the J-integrals in a cracked body. In Sect. 4, we focus on the crack faces and examine the role of the configurational surface forces on the crack faces. As we have previously explained the application of the configurational forces approach to fracture problems in considerable detail in previous papers by Simha et al. (2003, 2005, 2008), we merely summarize the results here.

2 The surface configurational force

As outlined in Fig. 2, we assume a region Ω that contains a bimaterial body B with a crack. The boundary of the region Ω is denoted as $\partial\Omega$. The external boundary of the body B, including the crack faces, is denoted

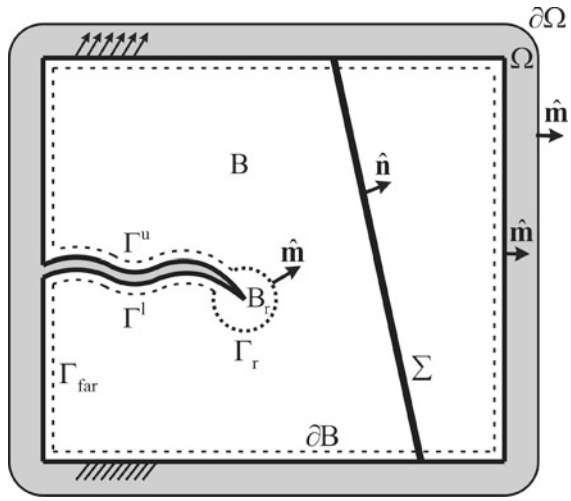

Fig. 2 The region Ω contains a bimaterial body B with a crack. The boundary of the region Ω is denoted as $\partial\Omega$. The external boundary of the body, including the crack faces, is ∂B. The bimaterial interface is Σ. The contour Γ_r encloses the crack tip at the boundary of the crack tip region B_r. The parameters $\hat{\mathbf{n}}$ and $\hat{\mathbf{m}}$ are the unit normal vectors to the interface Σ, or to the contours and boundaries, respectively. Matter of different type fill the gap between ∂B and $\partial\Omega$. The integration contours Γ^u and Γ^l along the crack faces and along the outer contour Γ_{far} of the body B are marked

as ∂B, which consists of the outer contour Γ_{far} and the parts Γ^{u} and Γ^{l} of the upper and lower crack faces. The bimaterial interface is Σ. The contour Γ_{r} with the radius r encloses the crack tip, forming the crack tip region B_{r}. Note that $\text{B}\backslash\text{B}_{\text{r}}$ tends to B (excluding the crack tip), if Γ_{r} shrinks to zero. The unit vector $\hat{\mathbf{n}}$ denotes the normal to the interface Σ, while $\hat{\mathbf{m}}$ denotes the outward unit normal vector to the external boundary ∂B, to the contour Γ_{r} of B_{r} and to the exterior boundary $\partial\Omega$. Matter of different type fills the gap between ∂B and $\partial\Omega$. No relevant singularity appears at the crack mouth, since the corners are considered as rounded.

The balance of deformational forces for a region Ω that contains a cracked body B without body forces (Fig. 2) requires

$$\int_{\partial\Omega} \mathbf{S}\hat{\mathbf{m}}\, dl = \mathbf{0}, \tag{1}$$

where $\mathbf{S}$ denotes the first Piola-Kirchhoff stress tensor. We ignore heat conduction and inertia for simplicity. A modified version of the divergence theorem that accounts for possible discontinuities at bimaterial interfaces, external boundaries and singular stress fields at the crack tip yields

$$\int_{\partial\Omega} \mathbf{S}\hat{\mathbf{m}}\, dl = \int_{\Omega} \nabla\cdot\mathbf{S}\, dA + \int_{\Sigma} [\![\mathbf{S}]\!]\,\hat{\mathbf{n}}\, dl + \int_{\partial\text{B}} [\![\mathbf{S}]\!]\,\hat{\mathbf{m}} dl + \lim_{r\to 0}\int_{\Gamma_{\text{r}}} \mathbf{S}\hat{\mathbf{m}}\, dl, \tag{2}$$

where ∇ is the Lagrangian gradient operator with respect to the coordinate vector $\mathbf{X}$ in the reference system and $[\![\mathbf{S}]\!]$ denotes the jump in $\mathbf{S}$ either at the bimaterial interface Σ or at the external boundary $\partial\mathbf{B}$, see the Appendices in Simha et al. (2003, 2005). Following the usual method for obtaining local relations in continuum mechanics, Eqs. (1) and (2) give

$$\nabla\cdot\mathbf{S} = \mathbf{0} \qquad \text{at each point in B or } \Omega, \tag{3}$$

$$[\![\mathbf{S}]\!]\,\hat{\mathbf{n}} = \mathbf{0} \qquad \text{at each point in } \Sigma, \tag{4}$$

$$[\![\mathbf{S}]\!]\,\hat{\mathbf{m}} = \mathbf{0} \qquad \text{at each point in } \partial\text{B}, \tag{5}$$

$$\lim_{r\to 0}\int_{\Gamma_{\text{r}}} \mathbf{S}\hat{\mathbf{m}}\, dl = \mathbf{0} \quad \text{at the crack tip.} \tag{6}$$

Equation (3) is the standard equilibrium equation of continuum mechanics; traction continuity on the interface Σ is ensured by Eq. (4) and on the external boundary ∂B by Eqs. (5), and (6) imposes restrictions on the nature of the singular stress field at the crack tip.

The total configurational force on a region Ω that contains a body B with a crack (Fig. 2) is

$$\int_{\Omega} \mathbf{f}\, dA + \int_{\Sigma} \mathbf{f}_{\Sigma} dl + \int_{\partial\text{B}} \mathbf{f}_{\text{S}} dl + \mathbf{f}_{\text{T}} + \int_{\partial\Omega} \mathbf{C}\hat{\mathbf{m}}\, dl = \mathbf{0}, \tag{7}$$

where the configurational stress $\mathbf{C}$ acts only at bulk points in Ω, but configurational forces are presumed to act at points in the bulk ($\mathbf{f}$), at the interface ($\mathbf{f}_{\Sigma}$), the external surface including the crack flanks ($\mathbf{f}_{\text{S}}$) and at the crack tip ($\mathbf{f}_{\text{T}}$). The bulk configurational stress $\mathbf{C}$ is nothing but the Eshelby- or energy-momentum tensor (see e.g. the derivation in Simha et al. 2003),

$$\mathbf{C} = \phi\mathbf{I} - \mathbf{F}^{\text{T}}\mathbf{S}, \tag{8}$$

where ϕ is the Helmholtz potential or the stored energy density, $\mathbf{I}$ is the identity tensor and $\mathbf{F}$ denotes the deformation gradient tensor ($\mathbf{F}^{\text{T}}$ is the transposed of $\mathbf{F}$).

Applying the modified version of the divergence theorem, Eq. (2) results with $\nabla|_{\text{expl}}$ being the divergence operator with respect to an explicit dependence on $\mathbf{X}$ (i.e. keeping the fields $\mathbf{F}$ and $\mathbf{S}$ fixed, see e.g. Maugin 2010) in the following:

$$\nabla|_{\text{expl}}\cdot\mathbf{C} + \mathbf{f} = \mathbf{0} \qquad \text{at each point in B or } \Omega, \tag{9}$$

$$[\![\mathbf{C}]\!]\,\hat{\mathbf{n}} + \mathbf{f}_{\Sigma} = \mathbf{0} \qquad \text{at each point on } \Sigma, \tag{10}$$

$$[\![\mathbf{C}]\!]\,\hat{\mathbf{m}} + \mathbf{f}_{\text{S}} = \mathbf{0} \qquad \text{at each point in } \partial\text{B}, \tag{11}$$

$$\lim_{r\to 0}\int_{\Gamma_{\text{r}}} \mathbf{C}\hat{\mathbf{m}}\, dl + \mathbf{f}_{\text{T}} = \mathbf{0} \qquad \text{at the crack tip.} \tag{12}$$

Equations (9), (10) and (12) agree with our previous derivations in Simha et al. (2003, 2005, 2008) and with other derivations in the literature, see Maugin (1993, 1995, 2010), Gurtin and Podio-Guidugli (1996), Gurtin (2000), Kienzler and Herrmann (2000), Steinmann (2000). In previous papers we did not focus on the entire external boundary of the cracked body, but examined only smooth crack faces with both faces considered as a single interface in the body. Also, we did not consider surface configurational forces along the crack faces explicitly as in Eq. (11) and instead assumed $[\![\mathbf{C}]\!]\,\hat{\mathbf{m}} = \mathbf{0}$ at the interface between the regions below and above the crack. As we will see below, for most situations the surface configurational force $\mathbf{f}_{\text{S}} = \mathbf{0}$, if the crack faces are smooth; then $[\![\mathbf{C}]\!]\,\hat{\mathbf{m}} = \mathbf{0}$ is consistent with Eq. (11). However, this needs not to be so necessarily. Therefore, in the current paper we explicitly consider surface configurational forces for the entire external boundary.

Typically the matter in the region outside the body (i.e. in $\Omega\backslash$B) will consist of one or more of the following: air or vacuum, rigid body, incompressible fluid, or compressible fluid. We now examine the configurational stress $\mathbf{C}$ and configurational body force $\mathbf{f}$ in the region outside the body (i.e. in $\Omega\backslash$B) for the different cases:

(a) Vacuum or air: Ignoring the negligible ambient pressure in air, we have $\phi = 0$ and $\mathbf{S} = \mathbf{0}$, hence we obtain $\mathbf{C} \equiv \mathbf{0}$ and consequently $\mathbf{f} = \mathbf{0}$.
(b) Rigid body: This would correspond to the grips of a loading device that impose displacement controlled boundary conditions. Here the stored energy density $\phi = 0$ and deformation gradient $\mathbf{F} = \mathbf{I}$, but the stress $\mathbf{S} \neq \mathbf{0}$; however, the stress is not related to the stored energy density and is instead determined from the solution of the equilibrium problem. We obtain $\mathbf{C} \equiv -\mathbf{S}$ and consequently $\mathbf{f} = \mathbf{0}$.
(c) Incompressible fluid: An example would be hydraulic fracturing. This is identical to the rigid body case.
(d) Compressible fluid: Here $\mathbf{C}$ would primarily be a function of density. If the fluid is homogeneous, then $\mathbf{f} = \mathbf{0}$. However, one has to be careful, if the fluid is inhomogeneous, since the configurational body force would not vanish identically then.

Consequently, for almost all situations that are encountered in structural fracture mechanics (meaning excluding the compressible fluid case), both the bulk configurational stress and the bulk configurational force in the material outside the fracture specimen vanish,

$$\mathbf{C} = \mathbf{0} \quad \text{and} \quad \mathbf{f} = \mathbf{0} \qquad \text{in } \Omega\backslash\text{B}. \tag{13}$$

Next we examine the surface configurational force $\mathbf{f}_\text{S}$ on the external boundaries of the body ∂B, which includes the crack faces. Eq. (11) can be re-written as

$$\begin{aligned}\mathbf{f}_\text{S} &= -[\![\mathbf{C}]\!]\,\hat{\mathbf{m}} = -\left(\mathbf{C}^\text{out} - \mathbf{C}^\text{in}\right)\hat{\mathbf{m}} \\ &= \left(\mathbf{C}^\text{in} - \mathbf{C}^\text{out}\right)\hat{\mathbf{m}}.\end{aligned} \tag{14}$$

$\mathbf{C}^\text{in}$ is the limiting value of $\mathbf{C}$, when ∂B is approached from inside the body B. $\mathbf{C}^\text{out}$ is the limiting value of the bulk configurational stress $\mathbf{C}$, when the external boundary ∂B is approached from outside the body (i.e. $\Omega\backslash$B). For regions of the boundary ∂B, where tractions are prescribed, they are induced by air or an incompressible fluid. Where displacements are specified, they are assumed to be transferred by a rigid body. Consequently $\mathbf{C}^\text{out} \equiv \mathbf{0}$, and Eq. (14) follows

$$\begin{aligned}\mathbf{f}_\text{S} &= \mathbf{C}^\text{in}\hat{\mathbf{m}} = \phi^\text{in}\hat{\mathbf{m}} - \left(\mathbf{F}^\text{in}\right)^\text{T}\mathbf{S}\hat{\mathbf{m}} \\ &= \phi^\text{in}\hat{\mathbf{m}} - \left(\mathbf{F}^\text{in}\right)^\text{T}\mathbf{t}.\end{aligned} \tag{15}$$

The (stress- or) traction vector $\mathbf{t} = \mathbf{S}\hat{\mathbf{m}}$ is the applied traction on parts of ∂B where traction is prescribed, or has to be determined from the solution of the equilibrium problem for regions where displacement is prescribed.

3 The surface configurational forces and J-integrals

We now determine the relation between the surface configurational forces on the external boundary ∂B and the J-integrals used in fracture mechanics. Consider the gray region D in Fig. 3, which contains the entire external boundary of the body, including the crack faces, but not the crack-tip region. The balance of configurational forces for the gray region D requires

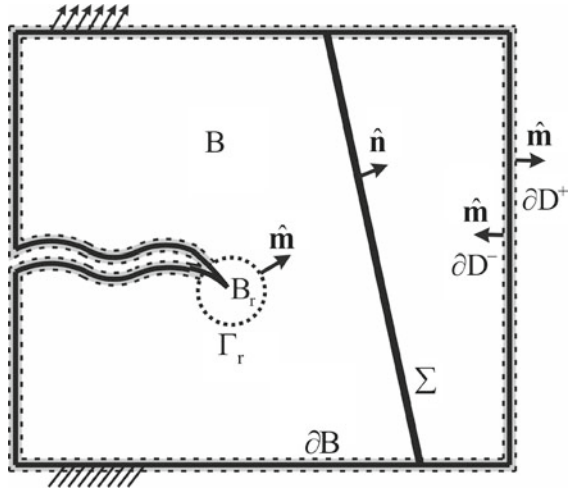

Fig. 3 The gray region D contains the entire external boundary of the body, including the crack faces, but not the crack-tip region. This region is used for relating the J-integral vector in the far-field and the surface configurational forces, Eq. (22)

$$\int_{D\cap(\Omega\setminus B)} \mathbf{f}\, dA + \int_{D\cap B} \mathbf{f}\, dA + \int_{\partial B} \mathbf{f}_S dl + \int_{\partial D} \mathbf{C}\hat{\mathbf{m}}\, dl = \mathbf{0}, \tag{16}$$

where the part of the gray region outside the fracture specimen is $D \cap (\Omega\setminus B)$, the part inside is $D \cap B$, and the traction due to the bulk configurational force acts on the boundary ∂D of the gray region. Next suppose that we collapse the gray region D in Fig. 3 to the external boundary ∂B. Then the first two integrals in Eq. (16) vanish, and the last integral can be written as

$$\int_{\partial D} \mathbf{C}\hat{\mathbf{m}}\, dl = \int_{\partial D^+} \mathbf{C}^{\text{out}}\hat{\mathbf{m}}\, dl + \int_{\partial D^-} \mathbf{C}^{\text{in}}\hat{\mathbf{m}}\, dl = \int_{\partial B} \mathbf{C}^{\text{out}}\hat{\mathbf{m}}\, dl - \int_{\partial B} \mathbf{C}^{\text{in}}\hat{\mathbf{m}}\, dl, \tag{17}$$

where the boundary $\partial D = \partial D^+ \cup \partial D^-$; the external normal to ∂D^- is opposite to the external normal on ∂B, hence the $-$ sign appears in front of the contour integral of $\mathbf{C}^{\text{in}}\hat{\mathbf{m}}$ on ∂B. Now Eq. (17) reduces to

$$\mathbf{J}_{\text{far}} - \mathbf{J}_{\text{out}} = \int_{\partial B} \mathbf{f}_S dl, \tag{18}$$

where we have used the following formal definitions of the J-integral vectors

$$\mathbf{J}_{\text{far}} = \int_{\partial B} \mathbf{C}^{\text{in}}\hat{\mathbf{m}}\, dl, \tag{19}$$

$$\mathbf{J}_{\text{out}} = \int_{\partial B} \mathbf{C}^{\text{out}}\hat{\mathbf{m}}\, dl. \tag{20}$$

If the region outside the body contains either vacuum, air, rigid material, or incompressible fluid, then Eq. (13) says that the bulk configurational force vanishes $\left(\mathbf{C}^{\text{out}} = \mathbf{0}\right)$; the only situation where this would not be true is the case, when the external region contains an inhomogeneous compressible fluid. Consequently for almost all cases encountered in structural applications, the J-integral vector in the external region vanishes identically,

$$\mathbf{J}_{\text{out}} = \mathbf{0}, \tag{21}$$

and we obtain the following relation between the J-integral vector in the far-field and the surface configurational forces

$$\mathbf{J}_{\text{far}} = \int_{\partial B} \mathbf{f}_S dl. \tag{22}$$

This means that the far-field J-integral vector can be obtained by integrating the surface configurational force over the entire external boundary of the body, which includes the crack faces, $\partial B = \Gamma_{\text{far}} + \Gamma^{\text{u}} + \Gamma^{\text{l}}$, but excludes the crack tip. We can readily recover the usual expression for the J-integral vector using Eq. (15) as

$$\mathbf{J}_{\text{far}} = \int_{\partial B} \mathbf{C}^{\text{in}}\hat{\mathbf{m}}\, dl = \int_{\partial B} \left[\phi^{\text{in}}\mathbf{I} - \left(\mathbf{F}^{\text{in}}\right)^{\text{T}}\mathbf{S}\right]\hat{\mathbf{m}}\, dl = \int_{\partial B} \left[\phi^{\text{in}}\hat{\mathbf{m}} - \left(\mathbf{F}^{\text{in}}\right)^{\text{T}}\mathbf{t}\right] dl. \tag{23}$$

The open literature and established software, such as ABAQUS (http://www.simulia.com/products/abaqus_fea.html), offer standard methods to evaluate the far-field J-integral as a scalar quantity, i.e. as projection of the J-integral vector $\mathbf{J}_{\text{far}}$ into the direction of crack propagation, $J_{\text{far}} = \mathbf{J}_{\text{far}}\cdot\mathbf{e}$, where $\mathbf{e}$ denotes the unit vector in crack growth direction, see below. Note that when computing the far-field J-integral with ABAQUS, not the outer contour ∂B is taken for the evaluation, but a contour Γ_{far} along the inward nodes of the elements situated along the outer boundary of the body. Moreover, Eq. (23) is not directly used; the J-integral values are calculated using the virtual crack extension method where the contour integral is transformed into an area integral (Parks 1977). Equation (22) provides a different, independent way of evaluating the far-field J-integral, if the surface configurational forces are provided by a postprocessor, e.g. Mueller et al. (2002, 2004), Shan (2008).

Lastly, we consider the region $B\setminus B_r$, assume a contour Γ_r at distance r from the crack tip, and form the limit $r \to 0$; this means finally the total region B excluding the crack tip. Now the balance of configurational forces reads

$$\int_{B\setminus B_r} \mathbf{f}\, dA + \int_{\Sigma} \mathbf{f}_\Sigma dl + \int_{\partial B} \mathbf{C}\hat{\mathbf{m}}\, dl + \int_{\Gamma_r} \mathbf{C}\left(-\hat{\mathbf{m}}\right) dl = \mathbf{0}. \tag{24}$$

The near-tip J-integral vector is written as

$$\mathbf{J}_{\text{tip}} = \lim_{r\to 0} \int_{\Gamma_r} \mathbf{C}\hat{\mathbf{m}}\, dl = -\mathbf{f}_T, \tag{25}$$

where $\mathbf{f}_T$ denotes the configurational force at the crack tip, Eq. (12). Then Eqs. (23)–(25) provide the relation

between the far-field and near-tip J-integral vectors for $r \to 0$ in the form

$$\mathbf{J}_{\text{tip}} - \mathbf{J}_{\text{far}} = \int_{\text{B}} \mathbf{f} dA + \int_{\Sigma} \mathbf{f}_{\Sigma} dl. \tag{26}$$

Since the crack faces are included in the far-field J-integral vector, the surface configurational forces on the crack faces do not appear explicitly in Eq. (26). Consequently, we get the important result that the surface configurational forces on crack faces are irrelevant to the difference between the near-tip and far-field J-integral vectors. However, in the formulation of Eq. (22) and, consequently, Eq. (26), the surface ∂B includes the crack surfaces but excludes the crack tip.

Finally, it is recalled from Simha et al. (2003, 2005, 2008) that the product $\mathbf{J}_{\text{tip}} \cdot \mathbf{v}_{\text{tip}}$ is the dissipation due to the crack tip moving with a velocity $\mathbf{v}_{\text{tip}}$. The crack driving force is the projection of the vector $\mathbf{J}_{\text{tip}}$ into the direction of $\mathbf{v}_{\text{tip}}$, i.e. the scalar quantity $J_{\text{tip}} = \mathbf{J}_{\text{tip}} \cdot \mathbf{e}$, where the unit vector $\mathbf{e} = \mathbf{v}_{\text{tip}}/|\mathbf{v}_{\text{tip}}|$ lies along the direction of crack growth.

4 Surface configurational forces on crack faces

4.1 General relations for the far-field J-integral vector

Intuitively, we expect the far-field J-integral vector $\mathbf{J}_{\text{far}}$ to be related to the applied loads in the far-field. Since loads can also be applied to the crack faces as in hydraulic fracturing or by wedge-loading at the crack mouth, the far-field contour would have to be the entire external boundary of a body. In particular, the far-field contour should include the crack faces as defined in Eqs. (20), (22) and (26). In contrast, typically the crack faces are not included in the far-field contours Γ_{far} for the evaluation of the far-field J-integral vector $\mathbf{J}_{\text{far}}$ or the scalar far-field J-integral J_{far}. To clarify this we rewrite Eq. (22) as

$$\mathbf{J}_{\text{far}} = \int_{\partial \text{B}} \mathbf{f}_{\text{S}} dl = \int_{\Gamma_{\text{far}}} \mathbf{f}_{\text{S}} dl + \int_{\Gamma^{\text{u}}} \mathbf{f}_{\text{S}} dl + \int_{\Gamma^{\text{l}}} \mathbf{f}_{\text{S}} dl. \tag{27}$$

Only if the integrals along the upper and lower crack faces Γ^{u} and Γ^{l} vanished, then it would be sufficient to use a contour like Γ_{far} that excludes the crack faces. Consequently, we now examine the value of the surface configurational forces on the crack faces for several scenarios below.

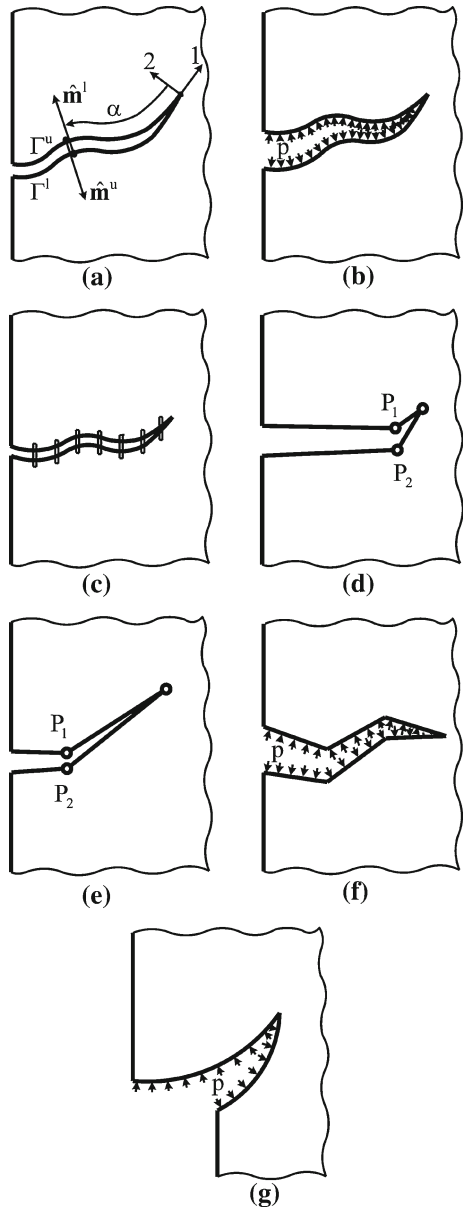

Fig. 4 Various crack configurations discussed in Sect. 4 for the examination of the surface configurational forces on the crack faces

4.2 Smooth and traction-free crack faces

Figure 4 shows a compilation of several representative crack configurations. Typically, the external unit normal vector to the upper crack face $\hat{\mathbf{m}}^{\text{u}}$ is opposite to the unit normal vector to the lower face $\hat{\mathbf{m}}^{\text{l}}$, which means $\hat{\mathbf{m}}^{\text{l}} = -\hat{\mathbf{m}}^{\text{u}}$ for a pair of opposing points that have the same arc-length from the crack tip, see Fig 4a. On a free

crack surface there is also no traction (either applied or reactions) present on the two crack faces $\left(\mathbf{t}^{\mathrm{u}} = \mathbf{t}^{\mathrm{l}} = \mathbf{0}\right)$. Under these circumstances, the surface configurational forces, Eq. (15), simplify to

$$\mathbf{f}_{\mathrm{S}} = \phi^{\mathrm{u}}\hat{\mathbf{m}}^{\mathrm{u}} \quad \text{on} \quad \Gamma^{\mathrm{u}} \quad \text{and} \quad \mathbf{f}_{\mathrm{S}} = \phi^{\mathrm{l}}\hat{\mathbf{m}}^{\mathrm{l}} \quad \text{on} \ \Gamma^{\mathrm{l}}. \tag{28}$$

In the context of linear elastic materials and for straight cracks (straight at least near the crack tip with the local coordinates (1, 2) in Fig. 4a), all components of the singular crack-tip stress vanish, $\sigma_{11} = \sigma_{12} = \sigma_{22} = 0$, on both the upper and lower crack faces for Mode I cracks, see e.g. Gross and Seelig (2006), Anderson (2004). Consequently, also the strain energy densities on the upper and lower crack faces vanish, i.e. $\phi^{\mathrm{u}} = \phi^{\mathrm{l}} = 0$ in the near-tip region for Mode I cracks. For Mode II cracks σ_{11} is equal and opposite for opposing points on the upper and lower crack faces (the stress components $\sigma_{12} = \sigma_{22} = 0$), but the strain energy densities are equal, i.e. $\phi^{\mathrm{u}} = \phi^{\mathrm{l}} \neq 0$. Similarly, for Mode III cracks, the out-of-plane shear stresses are equal and opposite on opposing points on the upper and lower crack faces, but the strain energy densities will be equal.

As a conclusion, for cracks with traction-free crack faces in elastic materials we obtain the following results for the surface configurational force $\mathbf{f}_{\mathrm{S}}$:

- For Mode I cracks, $\mathbf{f}_{\mathrm{S}} = \mathbf{0}$ identically everywhere on the upper and lower crack faces both in the near-tip region and in the far-field, so the contribution from each of the crack faces vanishes, i.e. $\int_{\Gamma^{\mathrm{u}}} \mathbf{f}_{\mathrm{S}} dl = \int_{\Gamma^{\mathrm{l}}} \mathbf{f}_{\mathrm{S}} dl = \mathbf{0}$. If the non-singular stresses have some non-zero components (e.g. if non-zero T-stresses occur in bend-type fracture mechanics specimens with small crack lengths or center cracked tension specimens, (Williams 1957; Anderson 2004), then $\mathbf{f}_{\mathrm{S}}$ is equal and opposite in sign at opposing points on the upper and lower crack faces, yielding
$$\int_{\Gamma^{\mathrm{u}}} \mathbf{f}_{\mathrm{S}} dl = -\int_{\Gamma^{\mathrm{l}}} \mathbf{f}_{\mathrm{S}} dl \neq \mathbf{0}. \tag{29}$$
- For Mode II and Mode III cracks, $\mathbf{f}_{\mathrm{S}}$ is equal and opposite in sign at opposing points on the upper and lower crack faces in the near-tip region and decays to a zero vector in the far-field. In any case, the contribution from each of the faces is equal and opposite in sign, so again Eq. (29) will be valid.

Consequently, the net contribution of the surface configurational forces from both crack faces vanishes in linear elastic materials for all three modes, since

$$\int_{\Gamma^{\mathrm{u}}+\Gamma^{\mathrm{l}}} \mathbf{f}_{\mathrm{S}} dl = \int_{\Gamma^{\mathrm{u}}} \mathbf{f}_{\mathrm{S}} dl + \int_{\Gamma^{\mathrm{l}}} \mathbf{f}_{\mathrm{S}} dl = \mathbf{0}. \tag{30}$$

In elastic-plastic materials, both the slip line solution and the Hutchinson-Rice-Rosengren (HRR) stress field near the crack tip have a non-zero stress σ_{11} on the crack faces for Mode I cracks, see e.g. Hutchinson (1968), Rice and Rosengren (1968) and Gross and Seelig (2006), Sect. 5.3 there. However, the strain energy density is the same at opposing points on the upper and lower crack faces. Consequently, Eqs. (29) and (30) will be valid also for Mode I cracks in elastic-plastic materials. Similar investigations can be performed for Mode II in elastic-plastic materials, but need a further investigation, being not the topic of this paper.

4.3 Smooth but non-zero traction crack faces

The traction vectors could either be applied traction vectors like in hydraulic fracturing (Fig. 4b), or reaction forces due to local contact of the crack faces, such as crack closure during cyclic loading, or due to crack-bridging fibers in composites (Fig. 4c). For many such cases, the traction will be equal but opposite in sign at opposing points on the upper and lower crack faces, i.e. $\mathbf{t}^{\mathrm{u}} = -\mathbf{t}^{\mathrm{l}}$. For symmetric or antimetric loading and a symmetric geometry with respect to the crack (i.e. crack lies in X-direction, normals to crack faces in Y-direction, Z-direction in out-of-plane direction; corresponding unit vectors $\mathbf{e}_X, \mathbf{e}_Y, \mathbf{e}_Z$; corresponding displacement vector $\mathbf{u} = u\mathbf{e}_X + v\mathbf{e}_Y + w\mathbf{e}_Z$), the resultant configurational force in two opposing points of the crack faces acts for Mode I and II in the crack-direction and for Mode III in the out-of-plane direction as

$$\text{Mode I} \quad \mathbf{t}^{\mathrm{u}} = t\mathbf{e}_Y: \quad \mathbf{f}_{\mathrm{S}}^{\mathrm{u}} + \mathbf{f}_{\mathrm{S}}^{\mathrm{l}} = -2t\frac{\partial v^{\mathrm{u}}}{\partial X}\mathbf{e}_X, \tag{31.1}$$

$$\text{Mode II} \quad \mathbf{t}^{\mathrm{u}} = t\mathbf{e}_X: \quad \mathbf{f}_{\mathrm{S}}^{\mathrm{u}} + \mathbf{f}_{\mathrm{S}}^{\mathrm{l}} = -2t\frac{\partial u^{\mathrm{u}}}{\partial X}\mathbf{e}_X, \tag{31.2}$$

$$\text{Mode III} \quad \mathbf{t}^{\mathrm{u}} = t\mathbf{e}_Z: \quad \mathbf{f}_{\mathrm{S}}^{\mathrm{u}} + \mathbf{f}_{\mathrm{S}}^{\mathrm{l}} = -2t\frac{\partial w^{\mathrm{u}}}{\partial Z}\mathbf{e}_Z. \tag{31.3}$$

The parameter t in Eq. (31) denotes the magnitude of the traction per length unit of the crack faces and unit thickness. These relations are also valid for cracks in elastic-plastic materials.

4.4 Non-smooth and non-zero traction crack faces

There are a few situations where Eq. (30) may not hold, as in the following:

- Traction-free crack faces but with kinks on the crack faces close to the crack tip (Fig. 4d). There can be an additional singularity at some of these kinks, see e.g. in P_2, Fig. 4d for a material angle $> \pi$, and Simha and Bhattacharya (1998), which would then appear as a non-zero surface configurational force. In general, $\mathbf{f}_S$ will have different values at kinks on the upper and lower faces and, hence, Eq. (30) may not be valid. The singular stress field at such a kink will likely influence the near-tip stress fields as well. However, if the kinks are in the far-field, the surface configurational force will likely be negligibly small (Fig. 4e).
- Applied tractions on crack faces plus kinks on crack faces (Fig. 4f). The stress field at some of these kinks could be singular, resulting in unequal, non-zero surface configurational forces on the upper and lower crack faces. Notice that any singularity at the crack mouth (like in the case of loading by a wedge at the crack mouth) would also fall under this case.
- Asymmetrical cracks plus applied tractions on crack faces (Fig. 4g): By asymmetry, we mainly mean that the consequence will be $\mathbf{F}^u \neq \mathbf{F}^l$. This could be the case, if there is a mixed-mode loading on the crack face; for a specific treatment, see e.g. Sect. 4.3 of the current paper and Kienzler et al. (2009).

However, for all these cases Eq. (30) may hold approximately, in the sense that the integrals in Eq. (30) may be vanishingly small in comparison to the magnitude of $\mathbf{J}_{far}$ for instance; this will be verified in future computational studies.

Some final remarks shall be made at the end of this section. For every case when Eq. (30) is valid, Eq. (27) reduces to

$$\mathbf{J}_{far} = \int_{\partial B} \mathbf{f}_S dl = \int_{\Gamma_{far}} \mathbf{f}_S dl. \tag{32}$$

Consequently, the current consensus practice of calculating the far-field J-integral on the contour Γ_{far} is valid for the vast majority of applications.

We consider it as important to note that the current derivation does not include any constitutive relation.

5 Numerical studies

Computational studies are conducted in order to evaluate (i) the relation between the far-field J-integral vector and the surface configurational forces, Eq. (22), and (ii) the influence of tractions on crack faces on the path dependence of the J-integral vector.

The modeling and computation of stresses, strains and energy densities are performed with ABAQUS (http://www.simulia.com/products/abaqus_fea.html). The configurational forces are calculated by a special post-processing procedure, see Simha et al. (2005, 2008), Kolednik et al. (2010), Shan (2008), Mueller et al. (2002, 2004).

5.1 Conventional fracture mechanics specimen, elastic-plastic material

As first example we investigate a homogeneous Compact Tension specimen with crack length $a = 27\,\text{mm}$, width $W = 50\,\text{mm}$, height $2H = 60\,\text{mm}$, compare Fig. 5. The material is a homogeneous elastic-plastic material with Young's modulus $E = 200\,\text{GPa}$, Poisson's ratio $\nu = 0.3$, yield strength $\sigma_y = 270\,\text{MPa}$, ultimate tensile strength $\sigma_u = 426\,\text{MPa}$, and strain hardening exponent $n = 0.2$, similar to a mild steel with German designation St37. Plane strain conditions are assumed for the computation. The finite element mesh consists of two-dimensional 4-node isoparametric elements. The elastic-plastic material behavior is modeled using the incremental plasticity model provided by ABAQUS. The specimen is loaded in Mode I by prescribing the displacement v_{LL} at the load application points (marked as LP in Fig. 5a) at the left boundary; no other traction forces exist. The material near the load application points is modeled as linear-elastic in order to avoid large artificial strains. Note that the specimen behaves as a homogeneous body as long as the plastically deformed zone does not touch this elastic region. The configurational forces are evaluated as outlined in Simha et al. (2008), Schöngrundner et al. (2010).

The distribution of the configurational forces for $v_{LL} = 0.25\,\text{mm}$ is depicted in Fig. 5. Note that somewhat modified configurational forces $\tilde{\mathbf{f}}_s$ are depicted. The reason is that considerable numerical errors may appear when calculating the configurational forces $\mathbf{f} = -\nabla|_{expl} \cdot \mathbf{C} = -\nabla|_{expl} \cdot \left(\phi \mathbf{I} - \mathbf{F}^T \mathbf{S}\right)$, Eq. (9), from the deformation gradient $\mathbf{F} = \mathbf{I} + \nabla \mathbf{u}$ for small

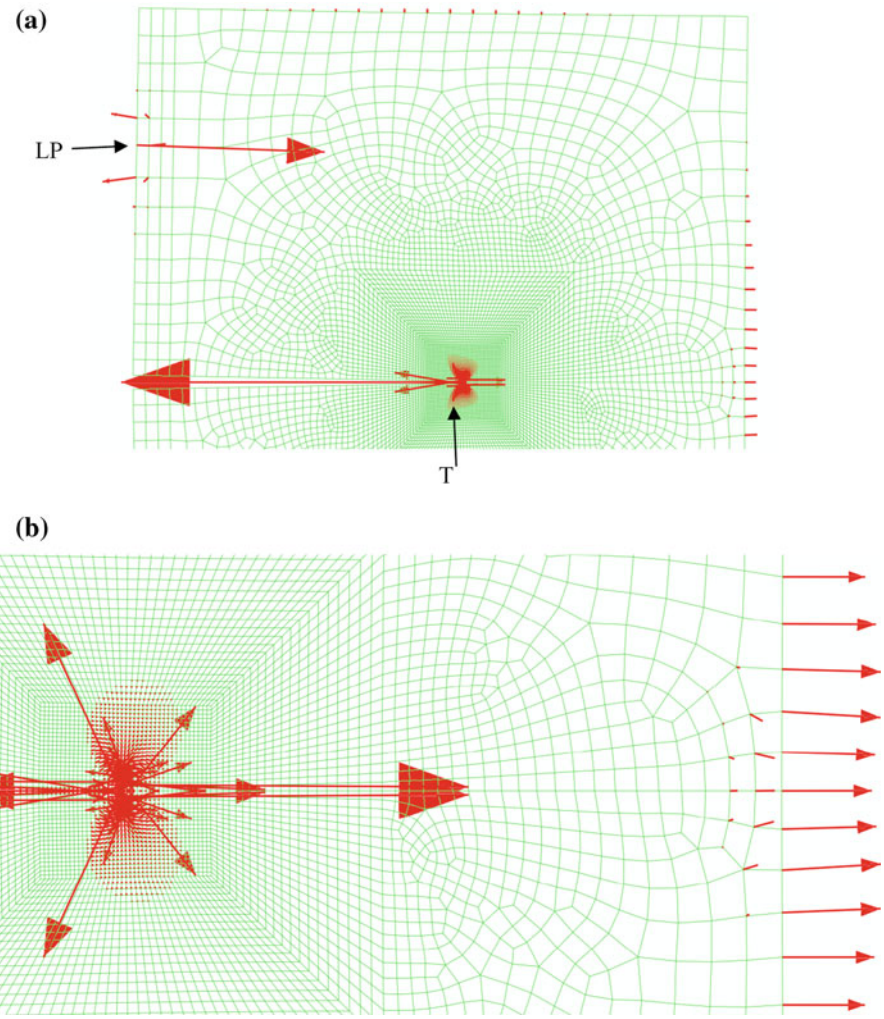

Fig. 5 Distribution of surface configurational forces $\tilde{\mathbf{f}}_s$ at the boundaries (*red arrows*) and configurational body forces in the interior (*red lines*) of a Compact Tension specimen. A large configurational force appears also at the crack tip T. **a** Overview of whole specimen; note the large horizontal configurational force at the load application point LP. **b** Detail near the crack tip

deformations. To avoid this, modified configurational forces are evaluated in the form $\tilde{\mathbf{f}} = -\nabla|_{\text{expl}} \cdot \tilde{\mathbf{C}} = -\nabla|_{\text{expl}} \cdot (\phi \mathbf{I} - \nabla \mathbf{u}^{\mathrm{T}} \mathbf{S})$ yielding $\nabla|_{\text{expl}} \cdot \tilde{\mathbf{C}} = \nabla|_{\text{expl}} \cdot \mathbf{C}$ everywhere in the body. The only difference appears regarding the surface configurational forces at the load application points where large traction vectors $\mathbf{t}$ appear. Then $\tilde{\mathbf{f}}_s = \mathbf{f}_s + \mathbf{t}$, and so the large vertical (and opposite) traction vectors in the load application points are omitted when plotting $\tilde{\mathbf{f}}_s$ instead of $\mathbf{f}_s$ in Fig. 5.

Bulk configurational forces appear due to the gradient of plastic strain within the plastic zone near the crack tip and near the back face of the specimen (Simha et al. 2008). Additional bulk configurational forces are visible near the load application points, but these are caused by numerical inaccuracies due to high local strains. Note that within a homogeneous elastic material no configurational body forces are expected. Surface configurational forces are present on the upper, right, lower and left parts of the external boundary, as well as on the crack faces. The surface configurational forces on the upper and lower boundaries and on the crack faces are small; they have no components in the horizontal 1-direction. In particular, notice that the values on the upper and lower crack faces are equal and opposite on a pair of opposing points on the two crack faces with the same distance from the crack tip.

Large surface configurational forces appear on the left boundary near the load application points and on the right boundary; in both cases, the components in the horizontal (1-) direction are considerably larger than those in the vertical (2-) direction. Together they deliver the main contribution to the total far-field J-integral

vector, which has a non-zero component in the horizontal direction. The vertical components of the surface configurational forces sum up to zero; hence the far-field J-integral vector has a zero vertical component.

These findings can be also deduced from Fig. 6, which presents the various contributions to the far-field J-integral vector $\mathbf{J}_{\partial B}$. Figure 6a collects the contributions with respect to the horizontal (1-) direction, Fig. 6b the contributions to the vertical direction. Shown are the J-integral components originating from the boundaries on the left ($\partial B - \ell$), right ($\partial B - r$), upper ($\partial B - u$) and lower ($\partial B - l$) sides of the specimen, as well as the contributions from the upper and lower crack faces, (CF − u) and (CF − l). Shown are, in addition, the near-tip J-integral vector $\mathbf{J}_{tip}$, which equals the negative configurational force at the crack tip $-\mathbf{f}_T$ (Eq. 25), the far-field J-integral vector $\mathbf{J}_{\partial B}$ evaluated from the whole boundary ∂B of the body (Eq. 22), as well as the scalar J-integral values $J_{\Gamma 3}$ and J_{far}, which are calculated along the path with a distance of 3 elements from the crack tip for Γ_3, i.e. a near-tip path, and the far-field path Γ_{far}, i.e. along the inner nodes of the outer boundary elements.

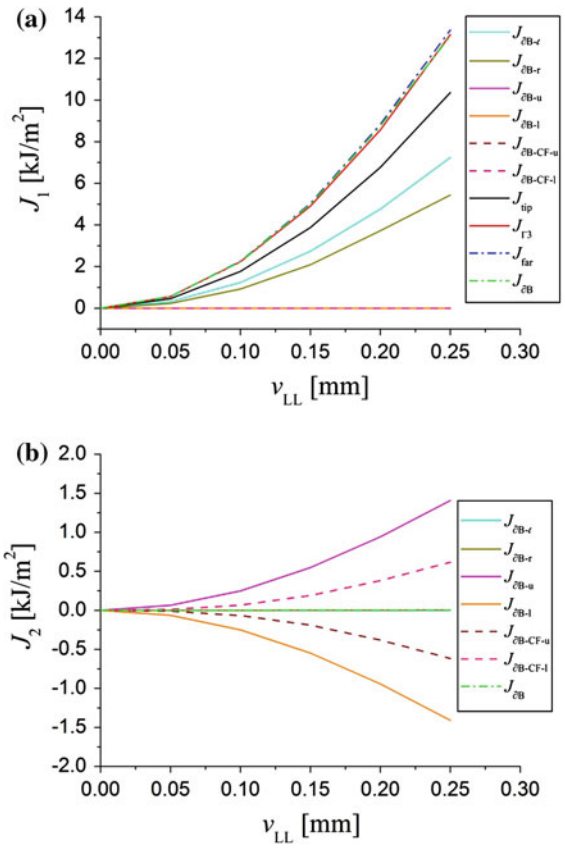

Fig. 6 Components of the J-integral vectors in **a** the horizontal (1-) direction and **b** the vertical (2-) direction, plotted against the load line displacement v_{LL}. The J-integral vectors are evaluated along the whole boundary ∂B of the body and along parts of the boundary on the *left* ($\partial B - \ell$), *right* ($\partial B - r$), *upper* ($\partial B - u$) and *lower* ($\partial B - l$) side, as well as on the *upper* and *lower* crack faces, (CF − u) and (CF − l). The near-tip J-integral vector $\mathbf{J}_{tip}$ equals the negative configurational force at the crack tip $-\mathbf{f}_T$, Eq. (25). $J_{\Gamma 3}$ and J_{far} are the values of the conventional, scalar J-integrals along the paths Γ_3 and Γ_{far}

An important observation in Fig 6a is that the scalar far-field J-integral, i.e. the projection of $\mathbf{J}_{\partial B}$ into the direction of the crack, calculated from the surface configurational forces according to Eq. (22), agrees closely with the standard contour integral J_{far} from ABAQUS. This provides evidence of the high accuracy of the numerical computations. The reader is also referred to the fact that the crack driving force J_{tip} differs from the scalar, far-field J-integral J_{far} due to plastic straining and incremental plasticity, which causes the occurrence of a non-zero plasticity influence term C_p, see Simha et al. (2008) for details.

5.2 Specimens with different loading cases, linear elastic material

As second example, we consider again a Compact Tension specimen ($a = 29$ mm, $W = 50$ mm, $2H = 60$ mm). The material behaves as linear elastic with $E = 210$ MPa and $\nu = 0.3$. Again plane strain conditions are assumed for the computations. Three different loading Cases are studied, namely

(i) Mode II loading by constant pressure $p = 100$ MPa between the crack faces;
(ii) Mode I loading by variable pressure between the crack faces, $p = p_{max}(1 - X/a)$ with $p_{max} = 200$ MPa; X is measured from the crack mouth towards the crack tip;
(iii) Mode II loading by constant shear stress $\tau = 100$ MPa on the upper and -100 MPa on the lower crack face.

Since neither a material inhomogeneity nor an elastic-plastic behavior exists, no configurational body forces appear and the J-integral vector is path independent, $\mathbf{J}_{far} = \mathbf{J}_{tip}$.

In the following, analytical expressions of the far-field J-integral vectors $\mathbf{J}_{\text{far}}$ shall be derived according to Eq. (23) for the three loading cases, compare also Eq. (27). No contribution to $\mathbf{J}_{\text{far}}$ arises from the upper ("u") and the lower ("l") boundaries, since no traction vector is acting there and since, due to symmetry, the elastic strain energy density ϕ has identical values, but opposite normal vectors $\hat{\mathbf{m}}$ at corresponding points on "u" and "l". No traction vectors are present also on the left ("ℓ") and right ("r") boundaries of the specimen, but the values of the elastic strain energy density ϕ will be significantly different at corresponding points on "ℓ" and "r", with opposite signs of the unit normal vectors $\hat{\mathbf{m}}$. The contributions of the upper and lower crack faces to $\mathbf{J}_{\text{far}}$ follow in straightforward way from Eqs. (31.1) and (31.2). With these considerations, the far-field J-integral vectors $\mathbf{J}_{\text{far}}$ follow as

$$\mathbf{J}_{\text{far}} = \left[\left(\int_{\text{r}} \phi ds - \int_{\ell} \phi ds \right) - 2 \int_{\Gamma^{\text{u}}} p\,(X)\, \frac{dv^{\text{u}}}{dX} dX \right] \mathbf{e}_X \tag{33}$$

for the Cases (i) and (ii) for constant and variable pressure and Mode I loading, resp., or as

$$\mathbf{J}_{\text{far}} = \left[\left(\int_{\text{r}} \phi ds - \int_{\ell} \phi ds \right) - 2 \int_{\Gamma^{\text{u}}} \tau \frac{du^{\text{u}}}{dX} dX \right] \mathbf{e}_X \tag{34}$$

for the Case (iii) for constant shear and Mode II loading.

Evaluation of the integrals Eqs. (33) and (34) yields after some analysis the following results for the X- and Y-components of the far-field J-integral vectors:

(i) constant pressure, Mode I

$$J_{\text{far},X} = \int_{-H}^{+H} (\phi_{\text{r}} - \phi_{\ell})\, dY + 2 p v_{\text{mouth}}, \qquad J_{\text{far},Y} = 0; \tag{35}$$

(ii) variable pressure, Mode I

$$J_{\text{far},X} = \int_{-H}^{H} (\phi_{\text{r}} - \phi_{\ell})\, dY + 2 p_{\max}\, (v_{\text{mouth}} - \bar{v})\,, \qquad J_{\text{far},Y} = 0; \tag{36}$$

(iii) constant shear, Mode II

$$J_{\text{far},X} = \int_{-H}^{H} (\phi_{\text{r}} - \phi_{\ell})\, dY + 2\tau\, u_{\text{mouth}}, \qquad J_{\text{far},Y} = 0. \tag{37}$$

In the equations above, u_{mouth} and v_{mouth} are the displacements of the upper crack face at the mouth of the crack, i.e., at $X = 0$, in horizontal (X- or 1-) and vertical (Y- or 2-) direction. The average value of the crack mouth displacement at the upper crack face in vertical direction is denoted in Eq. (36) as $\bar{v}$.

It is interesting to consider the contributions of the crack faces for a concrete numerical example for each of the three loading cases presented above. To do so, ABAQUS was used to calculate the deformation and stress state and the elastic strain energy ϕ. The integrals in Eqs. (35), (36) and (37) were then evaluated numerically by a postprocessor. The FE-computations were performed for both small and large strain setting, with practically no difference in the results. Therefore, only the results for small strain setting are used in the following. The results are collected in Table 1 under "Semi-analytical Solutions"; only the J-integral components in X-direction are listed. The term $J_{\partial \text{B}-\text{r}}$ denotes the contribution of the right vertical boundary to the far-field J-integral. $(J_{\partial \text{B}-\text{l}\ell} + J_{\partial \text{B}-\text{u}\ell})$ is the total contribution of the left boundary; hereby the contributions of the lower and upper specimen half are given separately. The term $(J_{\partial \text{B}-\text{CF}-\text{u}} + J_{\partial \text{B}-\text{CF}-\text{l}})$ denotes the contribution from the upper and lower crack faces.

As second way, the configurational force postprocessor to ABAQUS, Shan (2008), was engaged to calculate the distribution of the configurational forces along the different parts of the boundary of the specimen and calculate J_{far} from Eq. (27). The results are collected in Table 1 under "Numerical solutions". In addition, the standard numerical solutions of the J-integral J^{VCE} provided by the ABAQUS virtual crack extension procedure are listed in Table 1. Note that for elastic homogeneous materials the near-tip J-integral equals the far-field value, $J_{\text{tip}} = J_{\text{far}}$.

Figure 7 shows an overview and some details of the configurational force distribution for Case 2, i.e. the loading by variable pressure between the crack faces. The image in the center gives an overview about the whole specimen. Above are shown the configurational forces near the crack tip, below the configurational forces along the crack faces, and on the right the configurational forces at the right boundary of the specimen. Figure 8 presents the contributions to the far-field J-integral VCE vector from the various parts of the boundary. Figure 8a shows the components of the J-integral vectors in horizontal (1-) direction, Fig. 8b those in the vertical (2-) direction. It might be inter-

Table 1 Contributions to the X-component $J_{\mathrm{far},X}$ of the far-field J-integral in kJ/m^2, resulting from various regions along the external boundary

Loading case	Semi-analytical solutions				Numerical solutions				ABAQUS J^{VCE}
	$J_{\partial \mathrm{B-r}}$	$J_{\partial \mathrm{B-l}\ell} + J_{\partial \mathrm{B-u}\ell}$	$J_{\partial \mathrm{B-CF-u}} + J_{\partial \mathrm{B-CF-l}}$	$J_{\mathrm{far},X}$	$J_{\partial \mathrm{B-r}}$	$J_{\partial \mathrm{B-l}\ell} + J_{\partial \mathrm{B-u}\ell}$	$J_{\partial \mathrm{B-CF-u}} + J_{\partial \mathrm{B-CF-l}}$	$J_{\mathrm{far},X}$	$J^*_{\mathrm{tip},X}$
Constant pressure	16.020	$-0.334 - 0.334$	200·0.200	55.352	17.096	$-0.033 - 0.033$	36.300	53.334	56.030
Variable pressure	26.840	$-1.165 - 1.165$	$400 \cdot (0.262 - 0.149)$	69.710	28.646	$-0.386 - 0.386$	21.338+21.338	70.550	71.753
Constant shear	0.287	$-0.593 - 0.593$	200·0.043	7.701	0.292	$-0.653 - 0.653$	3.951+4.183	7.120	7.479

* $J_{\mathrm{tip},X} \equiv J_{\mathrm{far},X}$.

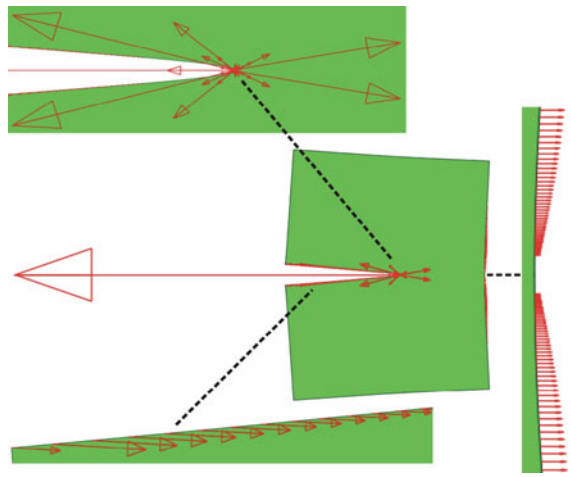

Fig. 7 Overview and some details of the distribution of the configurational forces for Case 2, i.e. loading by a linearly varying pressure p between the crack faces ($p_{\max} = 200\,\mathrm{MPa}$ at crack mouth, decreasing linearly to $p = 0$ at crack tip)

esting to compare these curves with the results listed in the second line of Table 1 under "Semi-analytical Solutions".

The results listed in Table 1 allow a comparison between the analytical procedure (columns referring to "Semi-analytical Solutions") and the results from the configurational forces postprocessor (columns referring to "Numerical solutions") and can be checked with the results from the ABAQUS VCE-procedure (last column). One can conclude as follows:

- All three ways to calculate J_{far} lead to similar results within "usual technical accuracy".
- The "Semi-analytical solutions" can be considered as the most accurate values. They use both displacements and elastic strain energy terms "far away" from the crack tip and, therefore, show the lowest dependency on mesh size and other numerical effects.
- The crack faces deliver the largest contribution to J_{far}, the left vertical boundaries the smallest contribution.
- The role of nonlinear geometrical behavior (large strain setting) can be taken into account, but has nearly no influence on the results for the actual case.

Finally, the reader is referred to the paper by Fischer et al. (2007), where (semi-) analytical J-integral solutions were studied, too, for several crack configurations, but without loading along the crack faces.

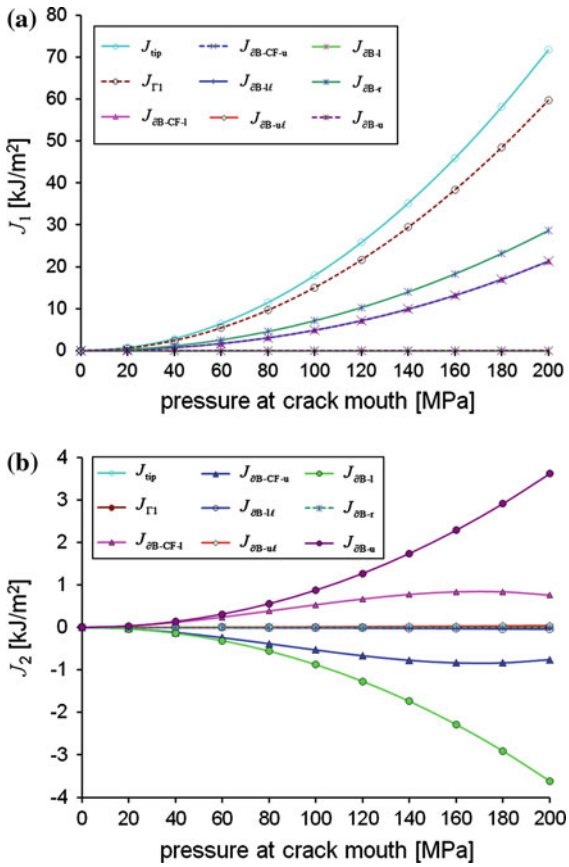

Fig. 8 Components of the J-integral vectors in **a** the horizontal (1-) direction and **b** the vertical (2-) direction. The J-integral vectors are evaluated at the crack tip $(\mathbf{J}_{\text{tip}} = \mathbf{J}_{\text{far}})$ and along parts of the boundary on the *left* ($\partial\text{B} - \ell$), *right* ($\partial\text{B} - \text{r}$), *upper* ($\partial\text{B} - \text{u}$) and *lower* ($\partial\text{B} - \text{l}$) side as well as on the *upper* and *lower* crack flanks ($\partial\text{B} - \text{CF} - \text{u}$, $\partial\text{B} - \text{CF} - \text{l}$). The contribution of the boundary on the left side is split into two components resulting from the upper and lower specimen part, $J_{\partial\text{B}-\text{u}\ell}$ and $J_{\partial\text{B}-\text{l}\ell}$, resp. Note that J_{tip} is the negative configurational force at the crack tip. $J_{\Gamma 1}$ is the value of the conventional, scalar J-integral along path Γ_1

6 Summary

The results of this paper can be summarized as follows:

(1) Expressions for the surface configurational forces have been derived and their values have been determined on regions of the external boundaries with prescribed tractions or displacements.
(2) The far-field J-integral vector $\mathbf{J}_{\text{far}}$ can be obtained by integrating the surface configurational forces over the entire external boundary of the body, which includes the crack faces, but excludes the crack tip.
(3) Only some special cases exist where the surface configurational forces along the crack faces give a contribution to the far-field J-integral vector $\mathbf{J}_{\text{far}}$. In many cases the contributions of the upper and lower crack faces are zero or cancel.
(4) The surface configurational forces on the crack faces do not alter the relation between the near-tip J-integral vector $\mathbf{J}_{\text{tip}}$ and far-field J-integral vector $\mathbf{J}_{\text{far}}$, i.e. the J-integral is path independent for elastic homogeneous materials.
(5) In our numerical examples where the specimens are loaded along the crack faces, the ABAQUS VCE-procedure give the correct values of the scalar far-field J-integral $\boldsymbol{J}_{\text{far}}$, however, there might exist some cases where this is not so.

Acknowledgments F.D.F. expresses his thanks to the valuable comments by Prof. H. Irschik, Johannes Kepler University Linz, Austria. Financial support by the Austrian Federal Government and the Styrian Provincial Government within the research activities of the K2 Competence Center "Integrated Research in Materials, Processing and Product Engineering", under the frame of the Austrian COMET Competence Center Programme, is gratefully acknowledged (Project A4.11-WP2).

References

Anderson TL (2004) Fracture mechanics: fundamentals and applications, 3rd edn. CRC Press, Boca Raton
Fischer FD, Predan J, Kolednik O, Simha NK (2007) Application of material forces to fracture of inhomogeneous materials: illustrative examples. Arch Appl Mech 77:95–112. Erratum (2008) 78:835
Gross D, Seelig T (2006) Fracture mechanics, with an introduction to micromechanics. Springer, Berlin
Gurtin ME, Podio-Guidugli P (1996) Configurational forces and the basic laws for crack propagation. J Mech Phys Solids 44:905–927
Gurtin ME (2000) Configurational forces as basic concepts of continuum physics. Springer, Berlin
Hutchinson JW (1968) Singular behavior at the end of a tensile crack tip in a hardening material. J Mech Phys Solids 16:13–31
Irschik H (2007) On rational treatments of the general laws of balance and jump, with emphasis on configurational formulations. Acta Mech 194:11–32
Kienzler R, Herrmann G (2000) Mechanics in material space. Springer, Berlin
Kienzler R, Rohde L, Schröder R, Kutz K (2009) Treating mixed-mode problems with path-independent integrals. In: Elboujdaini M et al. (eds) Proc 12th International Conference on Fracture (ICF12), paper T06.029, 10 p

Kolednik O, Predan J, Fischer FD (2010) Reprint of cracks in inhomogeneous materials: comprehensive assessment using the configurational forces concept. Eng Fract Mech 77:3611–3624

Maugin GA (1993) Material inhomogeneities in elasticity. Chapman & Hall, London

Maugin GA (1995) Material forces: concepts and applications. ASME Appl Mech Rev 48:213–245

Maugin GA (2010) Configurational forces: thermomechanics, physics, mathematics, and numerics. CRC Press, Boca Raton

Mueller R, Kolling S, Gross D (2002) On configurational forces in the context of the finite element method. Int J Numer Meth Eng 53:1557–1574

Mueller R, Gross D, Maugin GA (2004) Use of material forces in adaptive finite element methods. Comput Mech 33:421–434

Parks DM (1977) The virtual crack extension method for nonlinear material behavior. Comput Meth Appl Mech Eng 12:353–364

Rice JR (1968) A path independent integral and the approximate analysis of strain concentration by notches and cracks. ASME J Appl Mech 35:379–386

Rice JR, Rosengren GF (1968) Plane strain deformation near a crack tip in a power-law hardening material. J Mech Phys Solids 16:1–12

Schöngrundner R, Kolednik O, Fischer FD (2010) The configurational force concept in elastic-plastic fracture mechanics—instructive examples. Key Eng Mater 417-418:297–300

Shan GX (2008) Post-processing program for calculating the configurational forces with ABAQUS, internal report, K2 Competence Center "Integrated research in materials, processing and product engineering", Leoben, Austria

Simha NK, Bhattacharya K (1998) Kinetics of a phase boundary with edges and junctions. J Mech Phys Solids 46:2323–2359

Simha NK, Fischer FD, Kolednik O, Chen CR (2003) Inhomogeneity effects on the crack driving force in elastic and elastic-plastic materials. J Mech Phys Solids 51:209–240

Simha NK, Predan J, Kolednik O, Fischer FD, Shan GX (2005) Crack tip shielding or anti-shielding due to smooth and discontinuous material inhomogeneities. Int J Fract 135:73–93

Simha NK, Fischer FD, Shan GX, Chen CR, Kolednik O (2008) J-integral and crack driving force in elastic-plastic materials. J Mech Phys Solids 56:2876–2895

Steinmann P (2000) Application of material forces to hyperelastostatic fracture mechanics part I: continuum mechanical setting. Int J Solids Struct 37:7371–7391

Williams ML (1957) On the stress distribution at the base of a stationary crack. ASME J Appl Mech 24:109–114